1-2018

Production and Correlation of Reactive Oxygen and Nitrogen Species in Gas- and Liquid-Phase Generated by Helium Plasma Jets Under Different Pulse Widths

Zhijie Liu

Chunxi Zhou

Dingxin Liu

Dehui Xu

Wenjie Xia

See next page for additional authors

Authors

Zhijie Liu, Chunxi Zhou, Dingxin Liu, Dehui Xu, Wenjie Xia, Qingjie Cui, Bingchuan Wang, and Michael G. Kong

Production and correlation of reactive oxygen and nitrogen species in gas- and liquid-phase generated by helium plasma jets under different pulse widths

Zhijie Liu, Chunxi Zhou, Dingxin Liu, Dehui Xu, Wenjie Xia, Qingjie Cui, Bingchuan Wang, and Michael G Kong

---

Articles you may be interested in

Comparison between the water activation effects by pulsed and sinusoidal helium plasma jets
Physics of Plasmas **25**, 013520 (2018); 10.1063/1.5016510

Fluid modeling of radical species generation mechanism in dense methane-air mixture streamer discharge
Physics of Plasmas **25**, 013519 (2018); 10.1063/1.5016855

Control of radial propagation and polarity in a plasma jet in surrounding Ar
Physics of Plasmas **25**, 013505 (2018); 10.1063/1.5010993

Influence of driving frequency on discharge modes in the dielectric barrier discharge excited by a triangle voltage
Physics of Plasmas **25**, 013512 (2018); 10.1063/1.4998615

Perspective: The physics, diagnostics, and applications of atmospheric pressure low temperature plasma sources used in plasma medicine
Journal of Applied Physics **122**, 020901 (2017); 10.1063/1.4993710

Discharge mode transition and temporal-spatial evolution of an air-water plasma jet generated by pulsating DC power
Physics of Plasmas **24**, 123515 (2017); 10.1063/1.5008487

Production and correlation of reactive oxygen and nitrogen species in gas- and liquid-phase generated by helium plasma jets under different pulse widths

Zhijie Liu,[1,a)] Chunxi Zhou,[1] Dingxin Liu,[1] Dehui Xu,[1] Wenjie Xia,[1] Qingjie Cui,[1] Bingchuan Wang,[1] and Michael G Kong[1,2,3,a)]

[1]*State Key Laboratory of Electrical Insulation and Power Equipment, Centre for Plasma Biomedicine, School of Electrical Engineering, Xi'an Jiaotong University, Xi'an, Shaanxi 710049, People's Republic of China*
[2]*Frank Reidy Center for Bioelectrics, Old Dominion University, Norfolk, Virginia 23508, USA*
[3]*Department of Electrical and Computer Engineering, Old Dominion University, Norfolk, Virginia 23529, USA*

In this paper, we present the effects of the pulse width (PW) on the plasma jet's discharge characteristics, particularly focusing on the production and correlation of the reactive oxygen and nitrogen species (RONS) in gas- and liquid-phase. It is found that the length of plasma jet plume first increases before the PW of 10 μs, then gradually decreases and finally almost remains unchanged beyond 150 μs. The plasma bullet disappears after the falling edge of the voltage pulse at low PW, while it terminates far ahead of the falling edge of voltage pulse at high PW. This is mainly attributed to accumulation of space charges that lead to weakening of the reduced electric field with an increase of PW from low to high. More important, it is found that the excited reactive species, the positive and negative ions from plasma jet, and the concentrations of NO_2^- and NO_3^- in deionized water exposed to plasma j*et al*so display the first increasing and then decreasing change trend with increase of PW, while the concentration of H_2O_2 in water almost displays the linearly increasing trend. This mainly results from the formation of the H_3O^+ and HO_2^-, as well as their ion water clusters that can produce more OH radicals to be converted into H_2O_2, while the NO_2^- and NO_3^- in gas phase can transport into water and exist most stably in water. The water cluster formation at gas-liquid interface is an important key process that can affect the chemical nature and dose of aqueous RONS in water; this is beneficial for understanding how the RONS are formed in liquid-phase. *Published by AIP Publishing.* https://doi.org/10.1063/1.4999520

I. INTRODUCTION

Atmospheric pressure plasma jets (APPJs) have recently attracted considerable interest as an efficient source of highly reactive species for applications in materials processing and biological medicine.[1–4] As we know, the APPJs generate long plasma plumes (about 10 cm) in open space rather than in confined discharge gaps, which make it possible for direct treatments, and have no limitation on the size and shape of the treated objects.[5,6] Additionally, the APPJs have a relatively high electron temperature and a low gas temperature, and high energy electrons can produce chemically rich gasphase environments with reactive oxygen and nitrogen species (RONS), which are very important for applications such as plasma medicine.[7,8] However, the control of chemical reactions and the production of RONS in the plasma jet are difficult because the discharge is very unstable and easily transforms to filamentary discharge when the operating conditions are slightly changed; the filamentary discharge would lead to lethal danger to the living tissue due to the high current and local gas heating.[9,10] Therefore, it is essential to regulate and control the discharge parameters to investigate the discharge characteristics and modes of the plasma jet for the biomedical applications.

Our interest has been focused on regulating and controlling the plasma jet though the parameters of pulse voltage. Pulse width (PW) is one of the important parameters, and it can be used to control the discharge characteristics such as plasma jet length and plasma bullet propagation. Up to now, some works about the effect of PW on plasma jet characteristics have been reported by some groups.[11–17] Walsh *et al.* reported the impact of PW on the propagation velocity of the ionization front and found that the maximum discharge length occurs under PW of 3 μs.[13] Lu *et al.* investigated that the effects of PW on the propagation of plasma bullets in a pulsed plasma jet and found that, as PW increases up to 100 μs, the bullet propagates out from the nozzle with longer delay time. When the PW is increased to more than 100 μs, the delay time of the bullet propagating out from the nozzle becomes much shorter.[14,15] Uchida *et al.* clarified the effect of the voltage duty ratio on the production of reactive O atoms at a driving voltage frequency of 5 kHz.[17] Even though some diagnostic studies under different PWs have been conducted and the corresponding physical mechanism has been fully discussed and confirmed, these studies only focused on the propagation of plasma bullets in open air and

a)Authors to whom correspondence should be addressed: liuzhijie2010@163.com and mglin5g@gmail.com

the reports about the influence of PW on the production of RONS in gas- and liquid-phase have not yet been performed. In particular, the correlation of RONS between gas- and liquid-phase is still largely unknown. Understanding the source of reactive species in the liquid phase possesses profound and important significance in the subsequent biomedical applications, such as bacteria inactivation and cancer cell destruction.[1–7,18–20]

The main purpose of this study is to clarify the effects of the PW on the plasma jet's discharge characteristics, with particular focus on the production of the RONS in gas- and liquid-phase, which are desirable for biological medicine applications. For this purpose, we diagnosed the RONS by optical emission spectroscopy (OES), molecular beam mass spectrometer (MBMS), and microplate reader to analyze the correlation of RONS, transported from gas phase into liquid phase.

II. EXPERIMENTAL SETUP

Figure 1(a) shows a schematic illustration of the experimental setup of plasma jet source, which is made up of a coaxial needle-to-ring electrode configuration, of which the needle is a tungsten needle with a length of 10 cm and a diameter of 0.1 mm, and is connected to a high voltage pulse supply. The ring is a copper sheet of a length of 10 mm, located 10 mm from the open end of quartz tube (od.: 6 mm, id.: 4 mm), and serves as the grounded electrode. The needle electrode is covered by an insulating dielectric material (quartz glass) with a length of 50 mm (od.: 2 mm, id.: 1 mm) to make the plasma plume more diffuse and stable in the quartz tube. Helium (He) with high purity (5N) is controlled by a mass flow controller into the tube from gas inlet at a rate of 3 L/min. A homemade pulse generator with a rising time of approximate 40 ns is used to generate the plasma jet, and the PW is adjustable according to fixed value of pulse rate. The pulse voltage and pulse rate are fixed at 8 kV and

4 kHz in this study. The corresponding PW can be adjusted from 0.5 μs to 200 μs. The electrical characteristics are measured by a digital oscilloscope equipped with voltage/current probes (P6015A and P6021, Tektronix), and the OES is detected by an Andor SR-750i grating monochromator (grating grooving 1200 lines/mm). Photographs of the plasma plumes are taken by a camera(Nikon D7000) with an exposure time of 1 s, and time evolution of APPJ plume are obtained by an ICCD camera (PI-MAX3, Princeton Instruments) with an exposure time of 5 ns. A molecular beam mass spectrometer (MBMS, Hiden Analytical, Ltd.) system is used for detecting positively and negatively charged species in the He plasma jet. A Petri dish filled deionized water of 5 mL is put underneath the plasma jet for studying the plasma-liquid interaction, the distance between the tube nozzle and the face of water is 10 mm, and the some long-lived aqueous reactive species such as H_2O_2, NO_2^-, and NO_3^- are generated in water. The measured methods of the concentrations of aqueous H_2O_2, NO_2^-, and NO_3^- can been found in previous reports.[7,21,22]

III. RESULTS AND DISCUSSION

A. The discharge characteristics

The images of the plasma jet plume are displayed in Fig. 1(b) for different PWs from 0.5 μs to 200 μs. It is found that the length of plasma jet plume first increases before the PW of 10 μs, after that gradually decreases, and finally becomes almost unchanged after the PW of 150 μs. When the PW is longer than 10 μs, the controlling of PW does not affect the length of plasma jet plume. The change of plasma jet length is mainly attributed to more energy injection leading to stronger space electric field with increase of PW before 10 μs, so the plasma jet plume has a longer length. Further increasing PW can significantly increase the accumulation of the space charges on the tube wall to cause the formation of reverse electric field. This will weaken the reduced electric
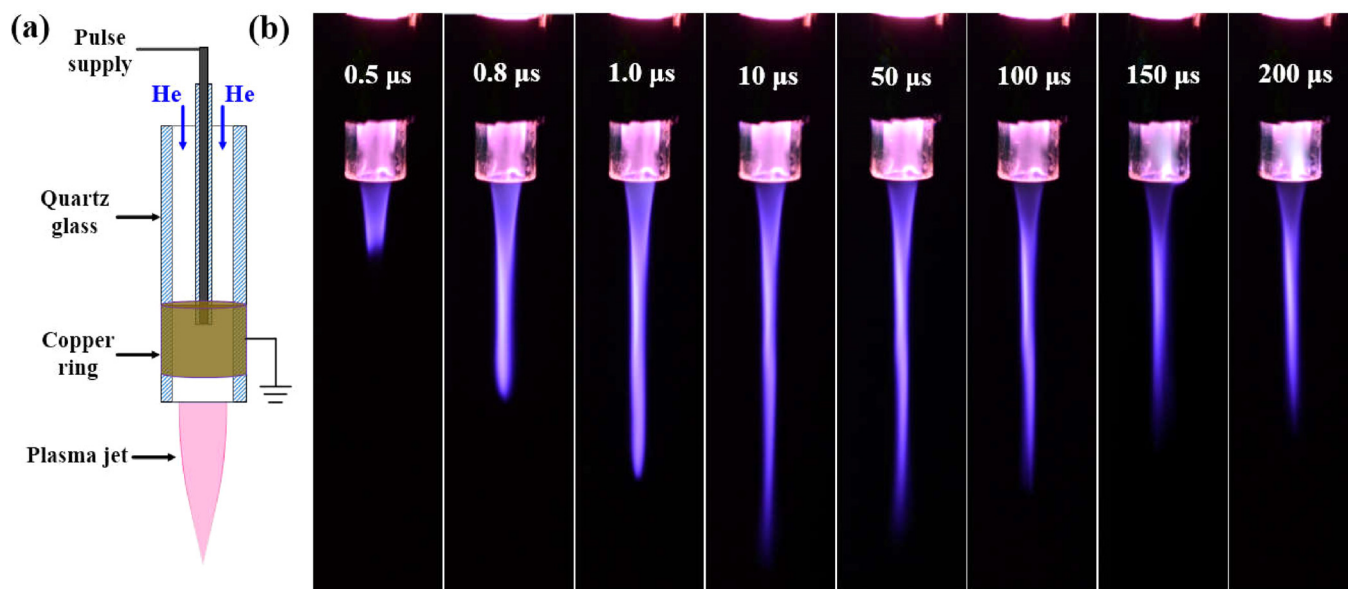

FIG. 1. (a) The schematic illustration of the experimental setup of plasma jet and (b) the images of plasma jet under different PWs at the pulse voltage of 8 kV, the pulse rate of 4 kHz, and the flow rate of 3 L/min.
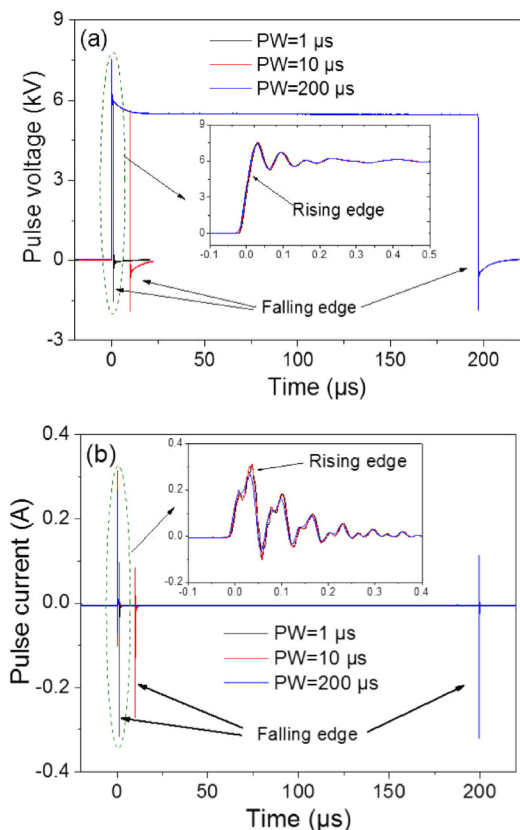
FIG. 2. The waveforms of (a) pulse voltage and (b) current of the plasma jet under different PWs of 1 μs, 10 μs, and 200 μs.

field in a discharge region, resulting in a shorter length of plasma jet plume compared to the length at PW of 10 μs.[15,23]

The typical waveforms of pulse voltage and current of the plasma jet are shown in Figs. 2(a) and 2(b) under PW of 1 μs, 10 μs, and 200 μs, respectively. It can be seen that the waveforms of pulse voltage at the rising edge almost overlap with each other. Except for their different PWs, the falling edge does as well. This implies that any change of the plasma jet plume is only caused by the PW, not by the other parameters of the pulse voltage supply. Additionally, it is also found that the waveforms of pulse current through the

grounded electrode has a positive pulse at the rise-edge of the voltage and a negative pulse at the fall-edge of the voltage. It is indicated that the plasma jet is only produced during the rise-edge and fall-edge phases as evidenced by the current peaks, similar to those reported pulse-excited discharges as a result of the reverse breakdown.[23,24]

To image the plasma jet plume on a nanosecond scale, the time-resolved images of the plasma jet under PW of 1 μs, 10 μs, and 200 μs are taken by ICCD camera and are shown in Fig. 3. The time of single pulse cycle (as shown in Fig. 2) is utilized to analyze the evolution behaviors of the plasma jet. It is found that the discharge behaviors for each PW of 1 μs, 10 μs, and 200 μs display plasma bullets, which start from initial breakdown within the tube and then propagate into the open air. Furthermore, as Figs. 3(a)–3(c) are compared with each other, the size of plasma bullet first increases, reaches the maximum size, then gradually decreases, and finally becomes smaller and darker until disappears as it propagates. For PW = 1 μs, the plasma bullet disappears after the falling edge of the voltage pulse; however, for PW = 10 μs and 200 μs, it is found that plasma bullet terminates far ahead of the falling edge of voltage pulse. Meanwhile, the existence of the plasma bullet for the PW = 10 μs starts from 0.74 μs to 2.34 μs and the interval is about 1.6 μs, which is significantly longer than the other cases (the 0.8 μs for PW = 1 μs, the 1.1 μs for PW = 200 μs), indicating that the duration of plasma bullet for the PW = 10 μs propagating in open air is the longest among of the three kinds of plasma jets. This may be explained by the accumulation of surface charge on the wall of tube; at the low PW (PW < 10 μs), the positive charges in the pulse cycle that propagates to the ground electrode will induce a polarization of the wall of tube, leading to the charges being deposited and forming the reverse electric field.[14,15] When the PW is increased from 0.5 μs to 10 μs, the more and more energy is input to the discharge system, and it leads to the higher reduced electric field and electron density produced in the discharge region. Correspondingly, more penning ionization takes place between the metastable He and the air molecules, and a longer plasma jet plume is produced.[14–17]
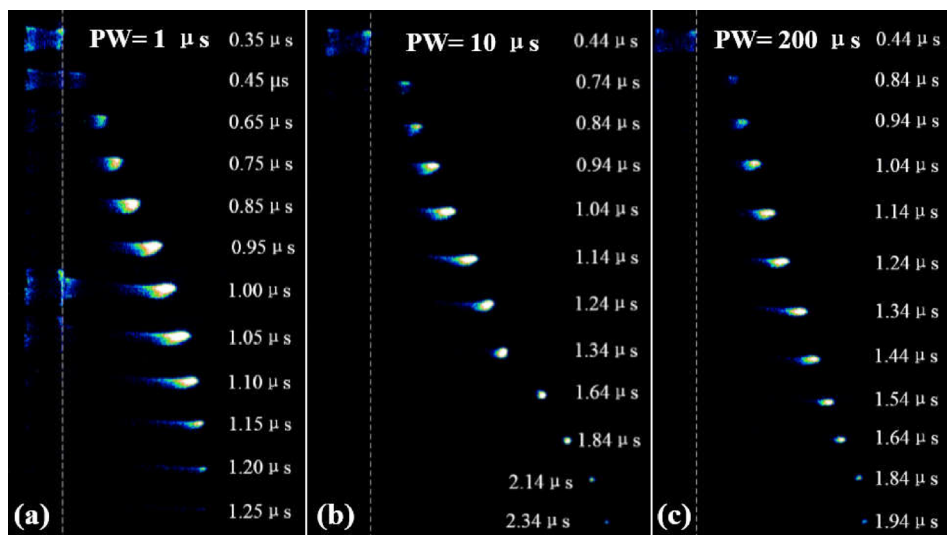

FIG. 3. The time-resolved images of the plasma jet under PW of 1 μs, 10 μs, and 200 μs, respectively.

However, continual increase of the PW (PW > 10 μs), on one hand, indicates the decrease in the voltage-off duration (pulse repetition rate of 4 kHz and pulse-cycle of 250 μs), and on the other hand, the energy input from pulse supply is not growing. The accumulated charged particles will perform a slow decay of electron-ion and ion-ion recombination in shorter voltage-off duration. The positive space charges are still deposited on the tube surface during the longer discharge duration.[14] These factors result in the reverse electric field increasing, and the reduced electric field is decreasing in the discharge region. So the appearance of the plasma bullet is delayed as shown in Fig. 3; the length of plasma jet plume and the size of the plasma bullets are becoming shorter and smaller until the accumulation of surface charges on the glass tube surface reach a saturated state.

B. The production of RONS in plasma jet

To identify and compare the reactive species from the plasma jet under different PWs, the OES in the wavelength range from 300 nm to 800 nm is shown in Fig. 4 at PW of 10 μs and 200 μs, respectively; the head of optical fiber is placed vertically to the axis of the tube at nozzle. From Fig. 4, it can be found that the emission spectra is mainly dominated by OH(A), N_2^+(B), He($3s^3$S), and O($3p^5$P) emissions; these reactive species produced are attributed to not only high energy electron excitation but also energy transfer from metastable He.[25] Additionally, these emission lines are almost the same for the plasma jets at PWs of 10 μs and 200 μs, while the emission intensity at PW of 10 μs is higher than that at PW of 200 μs. The similarity of emission lines indicates that these two kinds of plasma jets have similar ability to produce reactive species such as OH despite the different PW; the dissimilarity of emission intensity suggests that the plasma jet at PW of 10 μs has a higher value of reduced electric flied and can produce much greater concentration of reactive species on the tube nozzle. It also confirms the above analysis and explanation about the effect of the PW on the length of plasma jet plume in Fig. 1(b). In order to study the effect of PW on the concentration of reactive species when the PW is increased from 0.5 μs to 200 μs, the
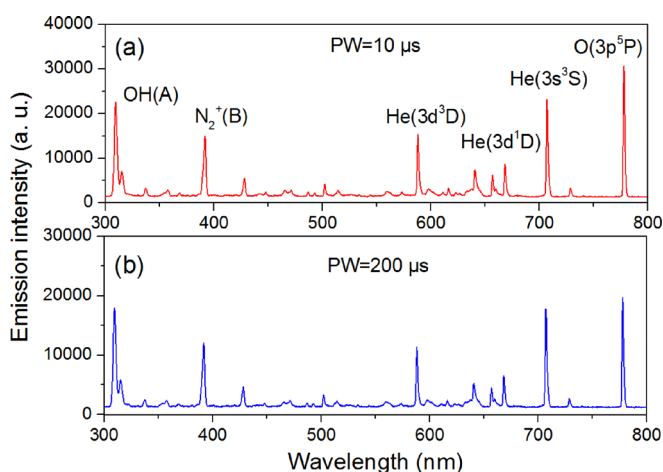
OES of reactive species OH(A), N_2^+(B), He($3s^3$S), and O($3p^5$P) from plasma jet at the exit of quartz tube are diagnosed at different PWs. The emission intensity of these species varying as a function of the PW is shown in Fig. 5. It is found that the emission intensity of OH(A), N_2^+(B), He($3s^3$S), and O($3p^5$P) first increases rapidly when the PW increases from 0.5 μs to 10 μs, and then decreases gradually with the increase of PW from 10 μs to 200 μs. The highest peak value for each is at 10 μs.

It is well known that when living tissues or cells are exposed to APPJs, the interactions between the reactive species and living tissues are believed to trigger a complex chain of biological reactions. Among the reactive species, the positive and negative ions also play an important role in biological medicine application. In our experiment, the molecular beam mass spectrometer is used for detecting the concentrations of positive and negative ions in He plasma jet. The instrument has a three-stage differentially pumped inlet system separated by aligned skimmer cones and pumps. Using the time-averaged intensities (counts/s), in the range 0–70 atomic mass units (amu), the positive and negative ions emanating from the plasma jets are identified. Figure 6 shows the time-averaged mass spectra of positive and negative ions from He plasma jet at PW of 10 μs. The plasma jet plume and sampling orifice are 15 mm apart. The assignment of mass spectrum peak for the m/z is also given in Fig. 6. It is found that nearly all peaks have been assigned except for the positive ions peak at m/z = 17 and the negative ions peaks at m/z = 19, 31, and 39, which may arise from some impurities. The positive and the negative ions mainly consist of N^+(m/z = 14), O^+(m/z = 16), N_2^+(m/z = 28), O_2^+(m/z = 32), OH^-(m/z = 17), O_2^-(m/z = 32), NO_2^-(m/z = 46), O_3^-(m/z = 48), and NO_3^-(m/z = 62), the general composition of ions is consistent with that of Bruggeman *et al.*[26] As reported in Refs. 26–29, the He^+ ions are produced inside the main discharge via electron neutral ionization process ($e^- + He \rightarrow 2e^- + He^+$). Major secondary ions (such as N_2^+ and O_2^+) in He plasma jet are mainly generated from direct electron impact ionization of air, penning ionization of N_2 by metastable He and charge exchange reactions of He^+ and

FIG. 4. The OES from the plasma jet at PW of 10 μs and 200 μs, respectively.
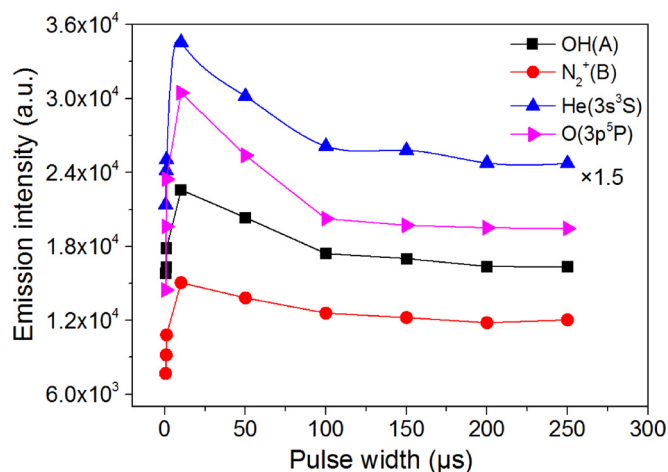
FIG. 5. The emission intensity of OH(A), N_2^+(B), He($3s^3$S), and O($3p^5$P) produced by plasma jet varies as a function of the PW.
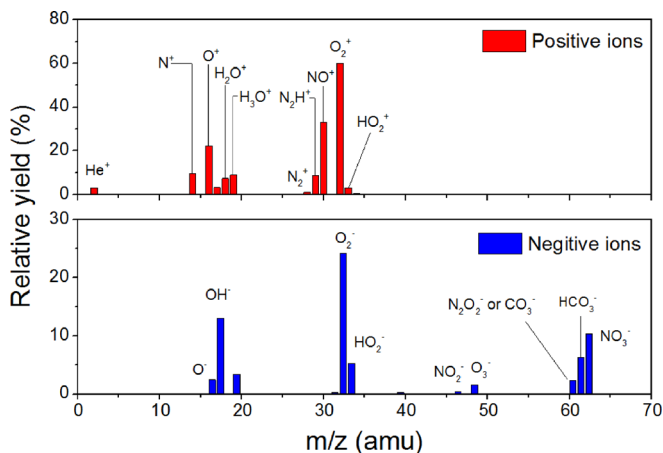
FIG. 6. The mass spectra of positive and negative ions from He plasma jet at PW of 10 μs measured in the outflow of the plasma jet at a distance of 15 mm from the gas nozzle.

He_2^+ with N_2 and O_2.[27,30] A large number of negative ions are obtained through the dissociative electron attachment ($e^- + AB \rightarrow A^- + B$) and further attachment process ($A^- + M \rightarrow A^- M$), where M denotes molecules in air.[26,27] Additionally, there are HO_2^- signals detected by mass spectrometry; it means that O_3^- and O_2^- ions may be converted to HO_2^- ions inside of this system.[31] And the peak of negative ion at $m/z = 60$ may be assigned to CO_3^- or $N_2O_2^-$.[28]

As reported in Refs. 26–33, among all positive ions generated by plasma jets in ambient air, hydronium ions (H_3O^+) are the dominant ions which reproduce to form water clusters. The positive ions generated by plasma jets would transfer their charges to hydronium ions if water molecules were abundant, such as in humid air or into water. Similarly, all negative ions generated by the plasma jets in ambient air, such as OH^-, HO_2^-, NO_2^-, and NO_3^-, would form water clusters stably.[26,27] For example, when the plasma jet is applied to a water surface, the density of water molecules is typically high near the water surface, and ion water clusters are formed. Furthermore, such water clusters are likely to dissolve directly into water to form the aqueous reactive species such as H_2O_2, NO_3^-, and NO_2^- when they reach the water surface.[34]

Figures 7(a) and 7(b) show the dependence of the PW on the relative yield of positive ions (N^+, O^+, N_2^+, O_2^+) and negative ions (OH^-, O_2^-, NO_2^-, NO_3^-), respectively. It is found that the relative yield of both positive ions and negative ions increase up to a maximum value at about 10 μs and gradually decrease for higher PW. The increase of relative yield with rising PW may be mainly ascribed to the increase of more energy input from the pulse voltage supply into the discharge region leading to a higher reduced electric field applied. However, when the PW is beyond to 10 μs, the number density of positive and negative ions begins to decrease because the more charges accumulated on the wall of a glass tube that form the reverse electric field result in the decrease of reduced electric field in gas gap.

C. The aqueous RONS production

As we know, APPJs contain a rich mixture of RONS, some of which include OH, O_2^-, H_2O_2, NO_2^-, and NO_3^-;
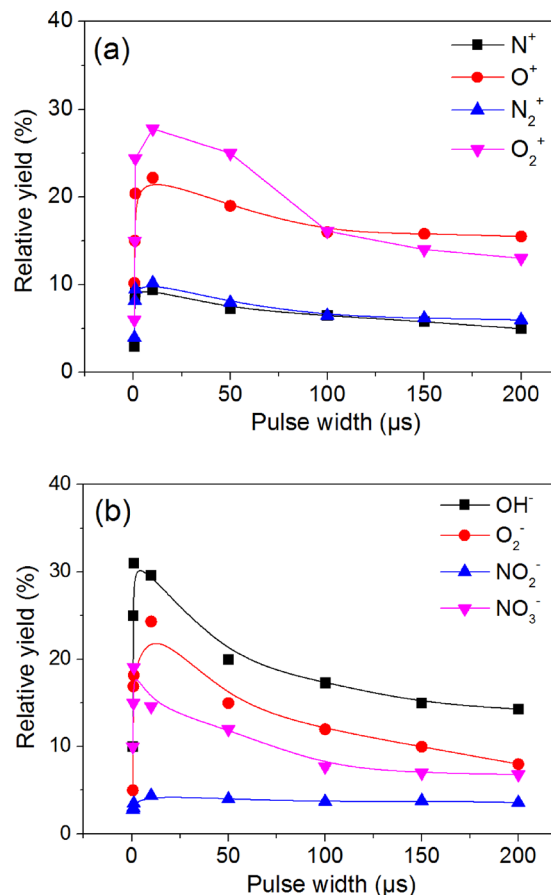

FIG. 7. The effect of the PW on the number density of positive ions for N^+, O^+, N_2^+, and O_2^+ (a) and negative ions for OH^-, O_2^-, NO_2^-, and NO_3^- (b).

these species in gaseous and liquid phases have been linked to biomedical effects such as bacteria inactivation and cancer cell destruction.[1,2,4,8] To confirm how the He plasma jet system generates some reactive species in deionized water, we measure the concentrations of H_2O_2, NO_2^-, and NO_3^- in water exposed to plasma jet under different PWs, and the results are shown in Fig. 8. It is shown that the H_2O_2 concentration in water almost increases linearly with the rising PW. It is well known that the OH is typically the main contributor to H_2O_2 production in both the gas and liquid phases,[21,34]
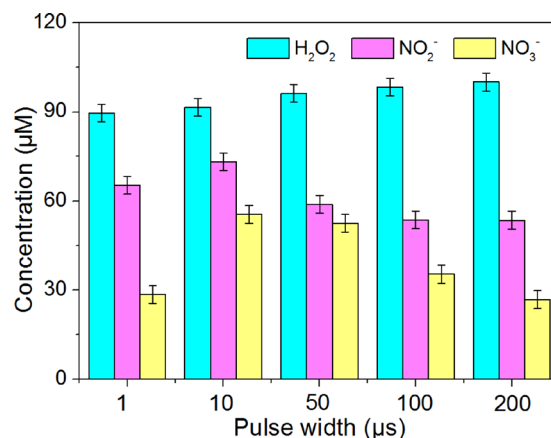

FIG. 8. The effect of PW on the concentrations of H_2O_2, NO_2^-, and NO_3^- in deionized water treatment by He plasma jet at different PWs.

while the concentrations of NO_2^- and NO_3^- in water display the first increasing and then decreasing trends, which are similar to the trends of NO_2^- and NO_3^- concentration in the gas phase in Fig. 7(b).

To dissect the correlation of RONS in the gas and liquid phases, the origins of H_2O_2, NO_2^-, and NO_3^- production in water are investigated further. For H_2O_2 production, there are three pathways. First, OH radicals are produced though traditional electron impact ionization of H_2O molecular. OH combines with other OH for H_2O_2 production in both the gas and liquid phases.[31–34] Second, it is known when water is exposed to He plasma jet, a series of complex chemical reactions (listed in Table I) take place above the gas-liquid interface. The presence of water vapour entrained in discharge results in increased reactions with H_2O. Positive ions (N_2^+ and O_2^+) produced in the gas phase react with H_2O, producing many OH radicals as in a series of chemical reactions from (1) to (12). Meanwhile, a large number of hydronium ions (H_3O^+) are formed as well as heavier ion water clusters ($H_3O^+(H_2O)_n$).[35] Third, negative ions HO_2^- and their water clusters ($HO_2^-(H_2O)_n$) dissolve into water, and then are quickly converted to other species.[36,37] For example, HO_2^- is the conjugate base of H_2O_2, and in an acidic environment, it can lead to additional H_2O_2 production. For the NO_2^- and NO_3^- production in water, on one hand, they originate from NO_2^- and NO_3^- ions in the gas phase. The NO_2^- and NO_3^- are the dominant negative ions that transport into water when the water is exposed to He plasma jet.[31] On the other hand, the NO, NO_2, and N_2O_5 in gas phase are also capable of reaching the gas-liquid interface and transported into water to form the aqueous NO_2^- and NO_3^- though complex chemical reactions from (13) to (18). The other negative ions are oxygen molecules such as O^-, O_2^-, and O_3^-, indicating

that the main pathway of creation is through dissociative electron attachment of O_2 and subsequent oxidization to form many of the negative ion species, as shown in the reaction from (19) to (21) in Table I.

In general, although mass spectrometry is so sensitive that it can detect very small quantities of gaseous ions, the observation shows that the concentrations of RONS generated by the plasma in the gas phase or at the gas-liquid interface are sufficiently high that they can affect the chemical nature of water that was exposed to the plasma.[38] The mass spectrometry data obtained in our study show that all dominant ion species generated by the plasma jet system contain either oxygen or nitrogen (N^+, O^+, N_2^+, O_2^+, OH^-, O_2^-, NO_2^-, NO_3^-), which suggests that the plasma generates a large amount of RONS. However, when plasma jet is applied to a wet surface (such as living tissues) or treated liquid, there is mainly ion water clusters formed near the surface. Additionally, there are many short-lived species (OH, O_2^-) and long-lived species (H_2O_2, NO_2^-, and NO_3^-) in the liquid.[39] It is believed that the water cluster formation (hydration process) at the gas-liquid interface can help us obtain more information about the correlation of RONS between in the gas phase and the liquid phase.

IV. CONCLUSIONS

In this paper, we studied the effects of the PW from $0.5\,\mu s$ to $200\,\mu s$ on the discharge characteristics of a plasma jet, with particular focus on the production and correlation of the ROS/RNS in gas- and liquid-phase, and the RONS are measured by OES, mass spectrometer, and microplate reader, respectively, for the purpose of analyzing and elucidating the correlation of RONS transported from gas phase into liquid phase. It is found that the length of plasma jet plume first increases before the PW of $10\,\mu s$, then gradually decreases, and finally becomes almost unchanged beyond $150\,\mu s$; this is mainly ascribed to the accumulation of space charges that lead to weakening of the reduced electric field with an increase of PW. Additionally, it is found that the excited reactive species, the positive and negative ions from plasma jet, and the concentrations of NO_2^- and NO_3^- in deionized water exposed to plasma j*et al*so display the first increasing and then decreasing change trend with increase of PW. However, the concentration of H_2O_2 in water increases almost linearly with the rising of PW, which is mainly attributed to the formation of the H_3O^+ and HO_2^-, as well as their ion water clusters that can produce more OH radicals to be converted into H_2O_2. The above results indicate that the water clusters generated by the plasma in the gas phase or at the gas-liquid interface are sufficiently high that they can affect the chemical nature and dose of aqueous RONS in water exposed to the plasma.

ACKNOWLEDGMENTS

TABLE I. The chemical reactions from plasma above water surface and in water.

No.	Chemical reactions	Refs.
(1)	$N_2 + e^- \rightarrow N_2^+ + 2e^-$	29
(2)	$N_2^+ + H_2O \rightarrow N_2H^+ + OH$	32
(3)	$N_2^+ + H_2O \rightarrow H_2O^+ + N_2$	32
(4)	$N_2H^+ + H_2O \rightarrow H_3O^+ + N_2$	33
(5)	$H_2O^+ + O_2 \rightarrow O_2^+ + H_2O$	33
(6)	$H_2O^+ + H_2O \rightarrow H_3O^+ + OH$	33
(7)	$H_3O^+ + H_2O + M \rightarrow H_3O^+(H_2O) + M$ with M=N_2, O_2	33
(8)	$O_2 + e^- \rightarrow O_2^+ + 2e^-$	32
(9)	$O_2^+ + H_2O + M \rightarrow O_2^+(H_2O) + M$ with M = N_2, O_2	33
(10)	$O_2^+(H_2O) + H_2O \rightarrow H_3O^+ + OH + O_2$ $\rightarrow H_3O^+(OH) + O_2$	33
(11)	$H_3O^+(OH) + H_2O \rightarrow H_3O^+(H_2O) + OH$	33
(12)	$e^- + H_2O + M \rightarrow H_2O^- + M$	35
(13)	$O_3 + NO_2^- \rightarrow O_3 + NO_3^-$	22
(14)	$2NO + 2HO_2 \rightarrow ONOOH \rightarrow H^+ + NO_3^-$	22
(15)	$NO_2 + O_2^- \rightarrow O_2 + NO_2^-$	22
(16)	$NO_3 + HO_2 \rightarrow NO_3^- + H^+ + O_2$	22
(17)	$NO_2 + OH \rightarrow NO_3^- + H^+$	22
(18)	$N_2O_5 + H_2O \rightarrow 2NO_3^- + 2H^+$	22
(19)	$e^- + 2O_2^- \rightarrow O + O^- + O_2$	22
(20)	$e^- + H_2O + O_2 \rightarrow H_2 + O^- + O_2$	22
(21)	$O + O^- + O_2 \rightarrow O_3^- + O$	22

[1] D. B. Graves, Plasma Process Polym. **11**, 1120–1127 (2014).

[2] P. Lukes, E. Dolezalova, I. Sisrova, and M. Clupek, Plasma Sources Sci. Technol. **23**, 015019 (2014).

[3] S. A. Norberg, E. Johnsen, and M. J. Kushner, Plasma Sources Sci. Technol. **24**, 035026 (2015).

[4] M. G. Kong, G. Kroesen, G. Morfill, T. Nosenko, T. Shimizu, J. Van Dijk, and J. L. Zimmermann, New J. Phys. **11**, 115012 (2009).

[5] X. Lu, Z. Jiang, Q. Xiong, Z. Tang, X. Hu, and Y. Pan, Appl. Phys. Lett. **92**, 081502 (2008).

[6] X. Lu, G. V. Naidis, M. Laroussi, and K. Ostrikov, Phys. Rep. **540**, 123–166 (2014).

[7] Z. J. Liu, D. H. Xu, D. X. Liu, Q. J. Cui, H. F. Cai, Q. S. Li, H. L. Chen, and M. G. Kong, J. Phys. D: Appl. Phys. **50**, 195204 (2017).

[8] D. T. EIg, I. W. Yang, and D. B. Graves, J. Phys. D: Appl. Phys. **50**, 475201 (2017).

[9] G. Uchida, S. Uchida, H. Kajiyama, and T. Shinoda, J. Appl. Phys. **107**, 023305 (2010).

[10] G. Uchida, K. Takenaka, and Y. Setsuhara, J. Appl. Phys. **117**, 153301 (2015).

[11] S. J. Kim and T. H. Chung, IEEE Trans. Plasma Sci. **39**, 2280 (2011).

[12] E. Robert, V. Sarron, D. Ries, S. Dozias, M. Vandamme, and J. M. Pouvesle, Plasma Sources Sci. Technol. **21**, 034017 (2012).

[13] J. L. Walsh, P. Olszewski, and J. W. Bradley, Plasma Sources Sci. Technol. **21**, 034007 (2012).

[14] Q. Xiong, X. Lu, Y. Xian, J. Liu, C. Zou, Z. Xiong, W. Gong, K. Chen, X. Pei, F. Zou, J. Hu, Z. Jiang, and Y. Pan, J. Appl. Phys. **107**, 073302 (2010).

[15] X. Lu, Z. Jiang, and Q. Xiong, IEEE Trans. Plasma Sci. **36**, 988 (2008).

[16] H. M. Joh, J. Y. Choi, S. J. Kim, T. H. Kang, and T. H. Chung, AIP Adv. **7**(8), 085106 (2017).

[17] G. Uchida, K. Takenaka, and Y. Setsuhara, Jpn. J. Appl. Phys., Part 1 **55**, 01AH03 (2016).

[18] K. C. Hsieh, R. J. Wandell, S. Bresch, and B. R. Locke, Plasma Process Polym. **14**, 1600171 (2017).

[19] D. B. Graves, Phys. Plasmas **21**, 080901 (2014).

[20] E. J. Baek, H. M. Joh, S. J. Kim, and T. Chung, Phys. Plasmas **23**, 073515 (2016).

[21] D. X. Liu, Z. C. Liu, C. Chen, A. J. Yang, D. Li, M. Z. Rong, H. L. Chen, and M. G. Kong, Sci. Rep. **6**, 23737 (2016).

[22] Z. C. Liu, D. X. Liu, C. Chen, D. Li, A. J. Yang, M. Z. Rong, H. L. Chen, and M. G. Kong, J. Phys. D: Appl. Phys. **48**, 495201 (2015).

[23] M. Z. Rong, W. J. Xia, X. H. Wang, Z. J. Liu, D. X. Liu, Z. H. Liang, X. N. Zhang, and M. G. Kong, Appl. Phys. Lett. **111**, 074104 (2017).

[24] Y. Xian, P. Zhang, X. P. Lu, X. K. Pei, S. Q. Wu, Q. Xiong, and K. Ostrikov, Sci. Rep. **3**, 1599 (2013).

[25] C. Zhang, T. Shao, Y. Zhou, Z. Fang, P. Yan, and W. Yang, Appl. Phys. Lett. **105**, 044102 (2014).

[26] P. Bruggeman, F. Iza, D. Lauwers, and Y. Aranda-Gonzalvo, J. Phys. D: Appl. Phys. **43**, 012003 (2010).

[27] J. S. Oh, Y. Aranda-Gonzalvo, and J. W. Bradley, J. Phys. D: Appl. Phys. **44**, 365202 (2011).

[28] M. Sabo, J. Páleník, M. Kučera, H. Han, H. Wang, Y. Chu, and S. Matejčík, Int. J. Mass Spectrom. **293**, 23 (2010).

[29] K. McKay, J. S. Oh, J. L. Walsh, and J. W. Bradley, J. Phys. D: Appl. Phys. **46**, 464108 (2013).

[30] T. Martensa and A. Bogaerts, Appl. Phys. Lett. **92**, 041504 (2008).

[31] T. Ito, K. Gotch, K. Sekimoto, and S. Hamaguchi, Plasma Med. **5**, 283 (2015).

[32] M. Pavlik and J. D. Skalny, Rapid Commun. Mass Spectrom. **11**, 1757 (1997).

[33] V. G. Anicich, J. Phys. Chem. Ref. Data **22**, 1469 (1993).

[34] T. Miura, A. Ando, K. Hirano, C. Ogura, T. Kanazawa, M. Ikeguchi, A. Seki, S. Nishihara, and S. Hamaguchi, J. Phys. D: Appl. Phys. **47**, 445402 (2014).

[35] C. A. J. vanGiles, S. Hofmann, and B. K. H. L. Boekema, J. Phys. D: Appl. Phys. **46**, 175203 (2013).

[36] J. D. Skalny, T. Mikoviny, S. Matejcik, and N. J. Mason, Int. J. Mass Spectrom. **233**, 317 (2004).

[37] K. Sekimoto and M. Takayama, Int. J. Mass Spectrom. **46**, 50 (2011).

[38] E. Stoffels, Y. Aranda Gonzalvo, T. D. Whitmore, D. L. Seymour, and J. A. Rees, Plasma Sources Sci. Technol. **16**, 549 (2007).

[39] J. D. Skalny, J. Orszagh, N. J. Mason, J. A. Rees, Y. Aranda-Gonzalvo, and T. D. Whitmore, Int. J. Mass Spectrom. **272**, 12 (2008).